ImmunoHorizons

RESEARCH ARTICLE

Innate Immunity

STAT1 Employs Myeloid Cell–Extrinsic Mechanisms to Regulate the Neutrophil Response and Provide Protection against Invasive *Klebsiella pneumoniae* Lung Infection

Shekina Gonzalez-Ferrer,[*,†,‡] Hernán F. Peñaloza,[*,†] Rick van der Geest,[*,†] Zeyu Xiong,[§] Atish Gheware,[§] Mohammadreza Tabary,[*,†] Megan Kochin,[*,†] Kathryn Dalton,[*] Henry Zou,[*] Dequan Lou,[*] Karina Lockwood,[*,†] Yingze Zhang,[*,†] William G. Bain,[*,†,¶] Rama K. Mallampalli,[‖] Anuradha Ray,[*] Prabir Ray,[*] Daria Van Tyne,[‡] Kong Chen,[*] and Janet S. Lee[*,†,§]

[*]Division of Pulmonary, Allergy, Critical Care, and Sleep Medicine, Department of Medicine, University of Pittsburgh, Pittsburgh, PA; [†]Acute Lung Injury Center of Excellence, Department of Medicine, University of Pittsburgh, Pittsburgh, PA; [‡]Division of Infectious Diseases, Department of Medicine, University of Pittsburgh, Pittsburgh, PA; [§]Division of Pulmonary and Critical Care Medicine, The John T. Milliken Department of Medicine, Washington University in St. Louis, St. Louis, MO; [¶]Veterans Affairs Pittsburgh Healthcare System, Pittsburgh, PA; and [‖]Division of Pulmonary and Critical Care Medicine, Department of Medicine, Ohio State University, Columbus, OH

ABSTRACT

Klebsiella pneumoniae (KP) is an extracellular Gram-negative bacterium that causes infections in the lower respiratory and urinary tracts and the bloodstream. STAT1 is a master transcription factor that acts to maintain T cell quiescence under homeostatic conditions. Although STAT1 helps defend against systemic spread of acute KP intrapulmonary infection, whether STAT1 regulation of T cell homeostasis impacts pulmonary host defense during acute bacterial infection and injury is less clear. Using a clinical KP respiratory isolate and a pneumonia mouse model, we found that STAT1 deficiency led to an early neutrophil-dominant transcriptional profile and neutrophil recruitment in the lung preceding widespread bacterial dissemination and lung injury development. Yet, myeloid cell STAT1 was dispensable for control of KP proliferation and dissemination, because myeloid cell–specific STAT1-deficient (*LysM*$^{Cre/WT}$;*Stat1*$^{fl/fl}$) mice showed bacterial burden in the lung, liver, and kidney similar to that of their wild-type littermates. Surprisingly, IL-17–producing CD4^{+} T cells infiltrated *Stat1*$^{-/-}$ murine lungs early during KP infection. The increase in Th17 cells in the lung was not due to preexisting immunity against KP and was consistent with circulating rather than tissue-resident CD4^{+} T cells. However, blocking global IL-17 signaling with anti–IL-17RC administration led to increased proliferation and dissemination of KP,

Received for publication January 8, 2024. Accepted for publication January 9, 2024.

Address correspondence and reprint requests to: Dr. Janet S. Lee, Division of Pulmonary and Critical Care Medicine, John T. Milliken Department of Medicine, Washington University in St. Louis, 660 South Euclid Avenue, MSC 8052-43-14, St. Louis, MO 63110-1093. E-mail address: ljanet@wustl.edu

ORCIDs: 0000-0002-0188-8844 (S.G.-F.); 0000-0002-1973-5934 (R.v.d.G.); 0009-0005-8628-7827 (H.Z.); 0000-0001-6947-2901 (Y.Z.); 0000-0001-7284-0103 (D.V.T.).

This work was supported by National Institutes of Health Grants P01HL114453, R01HL136143, R01HL142084, K24HL14285 (to J.S.L.), and F31HL165732 (to S.G.-F.) and by Career Development Award Number IK2 BX004886 from the U.S. Department of Veterans Affairs (to W.G.B.).

S.G.-F. and J.S.L. conceived and designed the research; S.G.-F., H.F.P., R.v.d.G., Z.X., A.G., M.T., M.K., K.D., K.L., Y.Z., and W.G.B. performed the experiments; S.G.-F., H.F.P., A.G., R.v.d.G., H.Z., D.L., W.G.B., D.V.T., K.C., and J.S.L. analyzed the data; S.G.-F., H.F.P., R.v.d.G., W.G.B., R.K.M., A.R., P.R., D.V.T., K.C., and J.S.L. interpreted the results of the experiments; S.G.-F. prepared the figures; S.G.-F. and J.S.L. drafted the manuscript; S.G.-F., H.F.P., R.v.d.G., Z.X., A.G., M.T., M.K., K.D., K.L., Y.Z., W.G.B., R.K.M., A.R., P.R., D.V.T., K.C., and J.S.L. edited and revised the manuscript; S.G.-F., H.F.P., R.v.d.G., Z.X., A.G., M.T., M.K., K.D., H.Z., D.L., K.L., Y.Z., W.G.B., R.K.M., A.R., P.R., D.V.T., K.C., and J.S.L. approved the final version of the manuscript.

The RNA sequencing data presented in this article have been submitted to the National Center for Biotechnology Information Gene Expression Omnibus (https://www.ncbi.nlm.nih.gov/geo/query/acc.cgi?acc=GSE251767) under accession number GSE251767 for bulk RNA sequencing and under accession number GSE252663 (https://www.ncbi.nlm.nih.gov/geo/query/acc.cgi?acc=GSE252663) for single-cell RNA sequencing.

Abbreviations used in this article: BALF, bronchoalveolar lavage fluid; BMDM, bone marrow–derived monocyte; GSEA, gene set enrichment analysis; KP, *Klebsiella pneumoniae*; NE, neutrophil elastase; PMN, polymorphonuclear; RNA-Seq, RNA-sequencing; scRNAseq, single-cell RNA sequencing; Treg, T regulatory cell; WT, wild type.

The online version of this article contains supplemental material.

https://doi.org/10.4049/immunohorizons.2300104

ImmunoHorizons is published by The American Association of Immunologists, Inc.

suggesting that IL-17 provided by other innate immune cells is essential in defense against KP. Contrastingly, depletion of $CD4^+$ T cells reduced *Stat1*$^{-/-}$ murine lung bacterial burden, indicating that early $CD4^+$ T cell activation in the setting of global STAT1 deficiency is pathogenic. Altogether, our findings suggest that STAT1 employs myeloid cell–extrinsic mechanisms to regulate neutrophil responses and provides protection against invasive KP by restricting nonspecific $CD4^+$ T cell activation and immunopathology in the lung.
ImmunoHorizons, 2024, 8: 122–135.

INTRODUCTION

Klebsiella pneumoniae (KP) is an extracellular Gram-negative bacterium that causes healthcare-associated and community-acquired infections such as lower respiratory tract infections, urinary tract infections, and sepsis. KP causes ∼12% of hospital-acquired pneumonia globally (1). KP virulence factors, including LPS and the polysaccharide capsule, are pathogen-associated molecular patterns that are recognized by pathogen recognition receptors expressed by immune and epithelial cells (2). Common pathogen recognition receptors, such as TLR4, can recognize pathogen-associated molecular patterns and trigger the master transcription factor NF-κB, which coordinates downstream inflammatory responses essential for host defense against pathogen invasion (3). STAT1 is a master transcription factor that is triggered by TLR signaling and is essential for the activation of types I, II, and III IFN signaling pathways (4–6). Deficiency of STAT1 is associated with combined insensitivity to IFN-I, -II, and -III (7). STAT1 is critical for antiviral as well as some antibacterial host defenses (4). We previously showed that STAT1 restricts extrapulmonary dissemination and sepsis in mice following acute intrapulmonary infection with KP (8), prompting a need to further investigate mechanisms involving STAT1 dysregulation (9–12).

Neutrophils are the initial infiltrating cells to combat bacterial pneumonia and prevent spread of infection to distant sites (13). Although neutrophils are essential for early and effective host defense against acute bacterial infection, an excessive neutrophil response can lead to tissue damage and injury (14). Previous studies in mice have demonstrated that STAT1 controls the buildup of neutrophils in conditions such as cancer and colitis-associated inflammation, presumably through suppression of IL-17 by STAT1 (15–17). This is consistent with the demonstrated role of STAT1 in controlling the differentiation of Th1 and Th17 cells (18). Although STAT1 loss-of-function mutations predispose individuals to infection (16, 17, 19, 20), STAT1 gain-of-function mutations lead to a state of autoimmunity and recurrent infections, in part because of impaired Th17 immunity (21, 22). It is notable that IL-17 itself plays a critical role in protective immunity against bacterial infections such as KP (23, 24), and *Il17r*$^{-/-}$ mice show increased mortality during KP pneumonia compared with controls and exhibit a significant reduction in neutrophil recruitment as well as increased extrapulmonary dissemination (25). In contrast, excessive IL-17 can promote inflammatory pathology in viral disease (23), including influenza (26). It is not known whether dysregulated IL-17 response can lead to immunopathology and tissue damage during lung infection with extracellular bacteria such as KP, although immunization-induced Th17 has been shown to be protective (27). The loss of types I, II, and III IFN signaling predisposes the host to severe immunosuppression; yet, *Stat1*$^{-/-}$ mice paradoxically show a propensity toward activation of effector $CD4^+$ or $CD8^+$ T cells and gut inflammation even in the absence of excess infection (7, 28, 29). Similarly, hyperinflammation has been reported in human subjects with loss-of-function mutations in STAT1, although this is poorly characterized functionally (7, 15, 30, 31). STAT1-mediated IFN-I and IFN-II restrain the activation of TCR-independent mechanisms in certain immunologic complications of cancer (32, 33). Still, others have reported that STAT1 acts to maintain T cell quiescence under homeostatic conditions and limits the bias toward Th17 cell skewing (7). Given prior reports of STAT1 in regulating neutrophil inflammatory response and maintaining T cell quiescence (7, 30, 34), in the present study, we examined whether the loss of STAT1 signaling could drive T cells, in particular $CD4^+$ T cells, toward a pathogenic state detrimental to host defense during infection and promote delayed lung injury.

MATERIALS AND METHODS

Animals

Stat1$^{-/-}$ mice [B6.129S(Cg)-*Stat1*^{tm1Dlv}/J mice, 012606] were originally obtained from The Jackson Laboratory and were backcrossed with C57BL/6J (000664) mice once to generate a colony at the University of Pittsburgh. Wild-type (WT) littermates and C57BL/6J mice, referred to as WT mice, were used as controls for *Stat1*$^{-/-}$ mice. *LysM*$^{Cre/WT}$;*Stat1*$^{fl/fl}$ mice were generated by crossing B6.129S-*Stat1*^{tm1Mam}/Mmjax (Mutant Mouse Resource & Research Centers strain 032054-JAX) with the LysMcre B6.129P2-*Lyz2*$^{tm1(cre)Ifo}$/J (004781; The Jackson Laboratory), and WT littermates (LysM$^{WT/WT}$;Stat1$^{fl/fl}$) were used as controls. All mice were fed a standard chow diet and were housed within the same room of the vivarium for at least 4 wk prior to experimentation. We used 8–16-wk-old age- and sex-matched mice for in vivo experiments, and trained personnel performed inoculations as well as organ harvests. All animals were housed and maintained in specific pathogen-free environments. Animal procedures were performed in compliance with the Guide for the Care and Use of Laboratory Animals from the National Research Council Institute for Laboratory Animal Research and were approved by the University of Pittsburgh Institutional Animal Care and Use Committee (IACUC protocols 23012117 and 21059260).

Experimental bacterial pneumonia model

A previously characterized KP clinical respiratory isolate called W42, which belongs to the hypervirulent K1 serotype (35), was used for all experiments. W42 was authenticated as KP and

https://doi.org/10.4049/immunohorizons.2300104

underwent multilocus sequence typing, capsular serotyping, and characterization of virulence genes by PCR (35). We previously showed that STAT1 deficiency leads to increased bacterial dissemination in mice intratracheally inoculated with the American Type Culture Collection 43816 strain (8). The W42 strain is more resistant to macrophage phagocytosis in vitro than the American Type Culture Collection 43816 strain (36). The W42 KP strain was grown in tryptic soy broth (TSB) overnight at 37°C with constant shaking at 250 rpm. One milliliter of overnight culture was inoculated in fresh TSB for a 1:100 dilution and grown for ∼1.5 h to reach an OD_{600} of 0.2. Bacterial cultures were harvested, washed, and resuspended in PBS before use. Mice were anesthetized with isoflurane, and 10^3 CFU of KP in a total volume of 100 μl was administered intratracheally under direct visualization using a sterile 200-μl pipet with the filtered tip positioned above the vocal cords. Bacterial inoculums were quantified by plating 10-fold serial dilutions on tryptic soy agar plates.

Bronchoalveolar lavage fluid collection

The trachea of each mouse was cannulated using a 20-gauge catheter secured with 2-0 silk suture. The left hilum was then identified and secured with 2-0 silk suture. Bronchoalveolar lavage fluid (BALF) collection was performed by instilling 0.6 ml 1× PBS, 0.6 mM EDTA, into the right lung, followed by three 0.5-ml washes for a total of 2.1 ml instilled. Total cell counts in BALF were determined using a hemocytometer. Cytospins were prepared from BALF and were stained with Diff-Quick (Siemens Healthcare Diagnostics). Differential cell counts were determined by counting a total of 200 cells per slide. The remaining BALF cells were pelleted by centrifugation at 400 × *g* for 15 min and aliquoted into cryovials for −80°C storage. The cell-free supernatant was subsequently used to measure total protein content (Pierce BCA protein assay kit; Thermo Fisher) and IgM measurement with frozen samples. Free neutrophil elastase (NE) activity was measured by placing fresh BALF aliquots in a clear 96-well plate with NE substrate (N-methoxysuccinyl-Ala-Ala-Pro-Val p-nitroanilide, 15 mM) with NaCl 5 M and Tris 1 M for 24 h. Absorbance was read at 410 nm at 0 h and 24 h. NE activity was calculated by subtracting OD_{410} 24 h from OD_{410} 0 h, and purified NE was used as the positive control.

Lung histology

In select experiments, following left lung ligation at the hilum with silk suture, the whole right lobe of the lung was inflated to 20 cm H_2O with 1% low melting agar using a digital traceable manometer (Fisher Scientific, catalog no. 06-664-18) or 2% paraformaldehyde using gravity. The lungs were dissected out of the thoracic cavity and then placed in ice-cold PBS for 1–2 min to solidify the agar. Lung lobes were cut away from each other and placed in a cassette containing 10% formalin. Lungs were maintained in solution at 4°C overnight and then transferred to 70% ethanol at 4°C prior to paraffin embedding followed by sectioning. Quantitative scoring of lung sections was performed using previously published guidelines (37).

Measurement of bacterial burden and cytokines and phagocytosis

The left lung, liver, and kidney were harvested immediately after euthanasia at predetermined time points. To enumerate bacterial CFU in the lung, liver, and kidney, the tissue was homogenized in 1 ml sterile ddH_2O. Next, 10 μl of tissue homogenates in triplicate were plated by 10-fold serial dilution on tryptic soy agar plates. Bacterial plates were counted after overnight incubation at 37°C and recorded as CFU/ml. Left lung tissue homogenates were also used for cytokine and chemokine analysis upon dilution with cytokine lysis buffer (0.5% Triton X-100, 150 mM NaCl, 15 mM Tris, 1 mM $CaCl_2$, and 1 mM $MgCl_2$, pH 7.4). Lung homogenates were diluted 1:5 for measurement of cytokines in ELISA plates, and the values in pg/ml were calculated on the basis of dilution. DuoSet ELISA kits (R&D Systems) were used to measure IL-1β, IL-6, IL-12p40, G-CSF, GM-CSF, and CXCL1 production according to the manufacturer's instructions. For additional cytokine measurements, lung homogenates were diluted 2:1 in 0.5% BSA in PBS, and cytokine levels were measured by multiplex immunoassay on a Bio-Plex 100 suspension array system (Bio-Rad Laboratories) and using the Bio-Plex Pro Mouse Cytokine 23-plex Assay (Bio-Rad Laboratories) according to the manufacturer's instructions. Bone marrow–derived monocytes (BMDMs) were isolated from WT and *Stat1*$^{-/-}$ mice and grown in DMEM with 20% FBS, 30% L929-conditioned medium, and 1% penicillin-streptomycin for ∼7 d at 5% CO_2 at 37°C to promote differentiation into macrophages as previously described (38). A phagocytosis assay was performed on WT and *Stat1*$^{-/-}$ BMDMs as previously described (36).

Klebsiella pneumoniae *ELISA*

An overnight KP culture was diluted in TSB 1:100 and shaken at 250 rpm, 37°C, for 2 h for the bacteria to reach log phase. Bacterial cells were pelleted and washed with sterile PBS twice and were then resuspended in 1/10 of the culture volume. Bacteria were heat killed at 95–100°C for 1 h and sonicated. The sonicated preparation was centrifuged at 17,000 × *g* for 15 min at 4°C, and the protein concentration of the supernatant (KP Ag) was measured by bicinchoninic acid assay (Pierce BCA protein assay kit; Thermo Fisher). The KP Ag was resuspended in carbonate buffer (1.36 g sodium carbonate, 7.35 g sodium bicarbonate, 950 ml H_2O, adjust pH to 9.2 with 1 M HCl or 1 M NaOH, if necessary, and add H_2O to 1 L) to a final concentration of 1 μg/100 μl. A Nunc MaxiSorp plate was coated with 100 μl KP Ag per well and incubated overnight. Afterward, the plate was washed with PBS containing 0.05% Tween-20 (PBS/T) four times and was then blocked with 250 μl/well PBS/T + 5% skim milk for 1 h at room temperature. Serial dilutions of convalescent serum from mice that recovered from KP infection were used as a positive control. After five subsequent washes with

PBS/T, 100 μl 1:1000 diluted goat anti-mouse IgG HRP-conjugated Ab (SouthernBiotech) in 5% milk was added to each well, and the plate was incubated at room temperature for 2 h. Washes were performed again five times prior to addition of 100 μl TMB color development solution (BD, 555214), and the plate was incubated at room temperature, checking development every 5–10 min. After 5–30 min, 50 μl stop solution (2 N H_2SO_4) was added to each well. Anti-KP IgG titers were determined by ELISA and reported in units obtained at OD_{450}.

Bulk RNA-sequencing and gene set enrichment analysis

Lungs were harvested from WT and *Stat1*$^{-/-}$ mice at 0 h or 24 h after intratracheal infection with 10^3 CFU of KP. RNA was purified from lung tissue using an RNeasy Plus Universal Mini kit (catalog 73407) according to the manufacturer's instructions (Qiagen), and purified RNA was sequenced by Novogene. Libraries were created using the Illumina platform, and paired-end reads were generated. RNA-sequencing (RNA-Seq) data were mapped against the mouse genomic sequence, gene sequence, and mRNA sequence. Differential expression analysis was performed using the DESeq software package (39, 40). Gene Ontology enrichment analysis of differentially expressed genes was implemented by the clusterProfiler R package. Gene Ontology terms with corrected p values <0.05 were considered to be significantly differentially expressed. Expression differences between treatment groups were considered significant when the absolute fold change was greater than or equal to 1.5, the maximum group mean was greater than or equal to 1, and the false discovery rate p value was <0.05. Data are illustrated using heatmaps, and the z-score was used to show differences across individual samples. Gene set enrichment analysis (GSEA) analysis was performed as previously outlined by Reimand et al. (39).

Single-cell RNA-Seq

Age- and sex-matched 12-wk-old *Stat1*$^{-/-}$ and WT mice were intratracheally inoculated with 5×10^3 CFU KP clinical isolate W42 grown to midlog phase. After 24 h, the mice were euthanized by an overdose of isoflurane. Uninfected age- and sex-matched naive mice served as untreated controls. Whole mouse lungs were digested with collagenase A and DNase I, then filtered through a 70-μm sterile cell strainer to generate single-cell suspensions. Neutrophils were depleted using Anti-Ly-6G MicroBeads (mouse) from Miltenyi Biotec. Cell viability was checked by Cellometer Auto 2000 Automatic Cell Viability Counter system (Nexcelom). A total of 5×10^3 live cells per sample were prepared for single-cell cDNA library construction with Chromium Next GEM Single Cell 5′ Reagent Kits version 2 (Dual Index) (10× Genomics). Viable single-cell suspensions were partitioned into nanoliter-scale Gel Beads-In-Emulsion. Full-length barcoded cDNAs were then generated and amplified by PCR for library construction. After enzymatic fragmentation, end-repair, A-tailing, and adaptor ligation, single-cell 5′ libraries were prepared for sequencing. The sizes of the single-cell RNA-Seq (scRNAseq) library pools were analyzed using a Standard Sensitivity NGS Fragment Analyzer Kit (Agilent). The libraries were then quantified by quantitative PCR on a LightCycler 480 (Roche) using the KAPA qPCR Quantification kit (KAPA Biosystems). The library pools were normalized per the manufacturer's protocol (Illumina). Sequencing was performed on the NovaSeq 6000 platform (Illumina) with 26 bp/90 bp paired-end reads on an SP-100 cycle flow cell version 1.5. Sequencing data were demultiplexed with 10× Genomics Cell Ranger mkfastq version 3.0.2. Basic processing of the scRNAseq data was performed with the Seurat package in R.

Flow cytometry and IL-17RC and CD4 depletion

Whole-lung tissues were harvested from WT and *Stat1*$^{-/-}$ mice. Single-cell suspensions were obtained following lung tissue digestion with collagenase (1 mg/ml) and DNase I (10 mg/ml) for 1 h at 37°C. For intracellular staining, cells were stimulated with PMA (1 μg/ml)/ionomycin (7.5 μg/ml) in GolgiStop for 4 h at 37°C prior to LIVE/DEAD cell staining and Ab labeling. To allow for dead cell exclusion, cells were washed twice with PBS and incubated with LIVE/DEAD Fixable Aqua Stain (Invitrogen, Thermo Fisher Scientific) in 1× PBS for 30 min at room temperature and protected from light. Cells were washed two times with PBS, immunostained for 30 min on ice while protected from light in cell staining buffer (PBS with 2% newborn calf serum) containing the following anti-mouse Abs: CD45-AF700 (clone 30-F11, BD Biosciences), CD45.2-AF700 (clone 104, BD Biosciences), CD11c-PE-cyanine (Cy)7 (clone HL3, BD Biosciences), Siglec-F-allophycocyanin-Cy7 (clone E50-2440, BD Biosciences), CD64-BV650 (clone X54-5/7.1, BD Biosciences), Ly6G-allophycocyanin (clone 1A8, BD Biosciences), CD24-BUV395 (clone M1/69, BD Biosciences), I-A/I-E-PerCP-Cy5.5 (clone M5/114.15.2, BD Biosciences), Ly6C-FITC (clone AL-21, BD Biosciences), MHC class II-PerCP-Cy5.5 (clone M5/114.15.2, BD Biosciences), CD3-BV421 (clone 17A2, BioLegend), CD19-BUV395 (clone 1D3, BD Biosciences), NK1.1-BV605 (clone PK136, BD Biosciences), CD49b-PerCP-Cy5.5 (clone DX5, BioLegend), TCRGammaDelta-PE (clone eBioGL3, eBioscience), TCRBeta-PE-CF594 (clone H57-597, BD Biosciences), CD4-PE-Cy5 (clone RMA4-5, BD Biosciences), CD8-BV480 (clone 53-6.7, BD Biosciences), CD69-allophycocyanin/Fire 750 (clone H1.2F3, BioLegend), CD103-BV785 (clone 2E7, BioLegend), and IL-17A-FITC (clone eBio17B7, Invitrogen). After staining, cells were washed twice in cell staining buffer and fixed overnight in 2% paraformaldehyde (Sigma-Aldrich) in PBS and stored at 4°C until the time of analysis (between 24 and 48 h). To obtain absolute cell counts, CountBright Absolute Counting Beads (Invitrogen, Thermo Fisher Scientific) were added to each sample before acquiring cells. For labeling circulating leukocyte studies, mice were administered CD45.2-AF700 Ab (1 μg/200μl/mouse; clone 104, BD Biosciences) via tail vein injection for i.v. delivery 3 min prior to lungs being harvested at 24 h postinfection (41). Following CD45.2 administration, we determined tissue-resident versus circulating cells based on a

method that was published previously (42). CD45.2^{pos} cells were considered i.v. positive and represented cells found in the circulation, whereas CD45.2^{neg} cells, or i.v. negative, were defined as cells within the lung interstitium or airspaces. For Ab depletion studies, mice were either administered 200 μg/mouse of anti-CD4 (clone GK1.5, Bio X Cell) at 48 h before infection or 50 μg/mouse of IL-17RC neutralizing Ab (Mouse IL17-RC Ab, catalog no. AF2270, R&D Systems) 6 h after infection with the respective IgG control Abs (clone LTF-2, Bio X Cell; and normal Goat IgG Control, catalog no. AB-108-C, R&D Systems). IL-17 production commences early after KP infection (~2 h), and therefore the 6-h time point was chosen for administration of anti–IL-17RC to provide sufficient levels of IL-17 to target (43). Cells were analyzed using a Cytek Aurora Spectral Flow Analyzer located in the unified flow core at the University of Pittsburgh, and data analysis was performed using FlowJo software (version 10; BD Biosciences) with a previously reported gating strategy for myeloid lineage cells (44) and the lymphoid gating strategy shown in Supplemental Fig. 1A.

Data accessibility

Data files for RNA-Seq reported in this paper have been deposited in the National Center for Biotechnology Information Gene Expression Omnibus under accession number GSE251767 (https://www.ncbi.nlm.nih.gov/geo/query/acc.cgi?acc=GSE251767) for bulk RNA-Seq and under accession number GSE252663 (https://www.ncbi.nlm.nih.gov/geo/query/acc.cgi?acc=GSE252663) for scRNAseq.

Statistics

The results are reported as median values unless otherwise stated; horizontal lines within graphs represent median values. Data are shown from one independent or multiple combined experiments and is stated within the figure legends. Dots within each representative graph demonstrate an individual mouse. A Shapiro–Wilk normality test was performed on the residuals of the data to evaluate whether the data followed a normal distribution. Significance was assessed using a nonparametric Mann–Whitney *U* test and was undertaken for in vivo comparisons between two groups as considered for when data did not follow a normal distribution. Two-way ANOVA was used for group comparisons over time. No outliers were excluded from the data. GraphPad Prism version 9 software was used for statistical analysis. A *p* value less than 0.05 was considered statistically significant.

RESULTS

STAT1 controls local pulmonary pathogen burden, extrapulmonary dissemination, and lung injury during Klebsiella pneumoniae*–induced sepsis*

We previously identified *Stat1* as a key regulator in host responses to acute pulmonary KP infection in the setting of heme-iron overload (45). To investigate the broader role of STAT1 in regulating the host response to KP intrapulmonary infection, we infected WT and *Stat1*$^{-/-}$ mice with KP and monitored the progression of infection over time following intratracheal inoculation with a clinical KP respiratory isolate (Fig. 1). At the early time point of 24 h after infection, WT and *Stat1*$^{-/-}$ mice showed similar lung bacterial burdens (Fig. 1A) and minimal, if any, extrapulmonary dissemination (Fig. 1B, 1C). By 48 h after infection, however, *Stat1*$^{-/-}$ mice showed increased bacterial burden compared with WT in the lung (Fig. 1A), liver (Fig. 1B), and kidney (Fig. 1C) that persisted at 72 h after infection. In addition, *Stat1*$^{-/-}$ mice showed increased lung microvascular permeability, as evidenced by increased BALF total protein concentrations (Supplemental Fig. 1B) and IgM levels (Supplemental Fig. 1C). Interestingly, Stat1$^{-/-}$ mice displayed increased BALF free NE activity (Supplemental Fig. 1D), suggesting higher neutrophil activation status than WT control mice. Histological examination as well as BALF polymorphonuclear (PMN) cell counts at 72 h also supported an exaggerated inflammation by 72 h after infection in the lungs of *Stat1*$^{-/-}$ mice (Supplemental Fig. 1E–1G). Together, these data indicate that *Stat1*$^{-/-}$ mice show impairments in bacterial

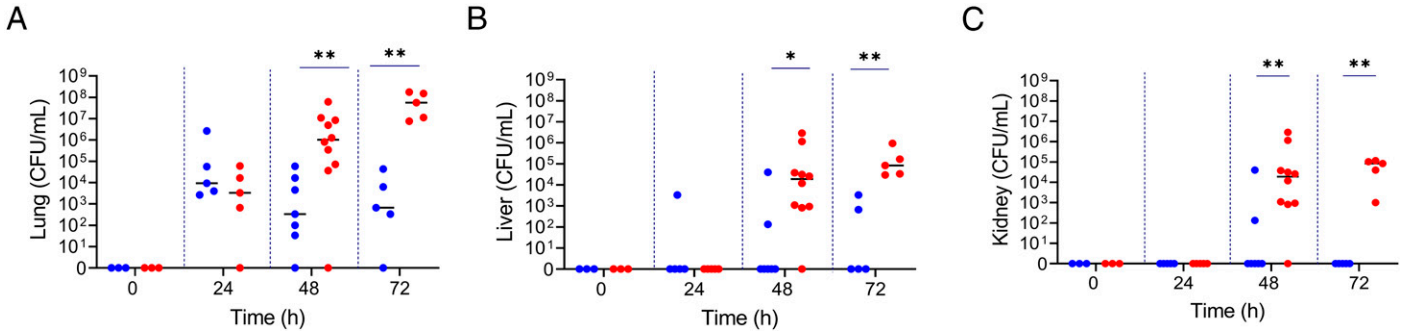

FIGURE 1.

Stat1$^{-/-}$ mice show delayed impairments in bacterial control of KP infection in the lung with widespread dissemination by 48 and 72 h after infection. Mice were infected intratracheally with 10^3 CFU of a clinical KP respiratory bacterial isolate, and CFUs were quantified in (**A**) lung, (**B**) liver, and (**C**) kidney homogenates at the indicated time points. Time 0 h represents naive, uninfected mice. Blue, WT; red, *Stat1*$^{-/-}$. Each dot represents an individual mouse. Horizontal lines indicate median values. *$p < 0.05$, **$p < 0.01$ from individual Mann–Whitney *U* tests.

control at both pulmonary and extrapulmonary sites and delayed lung injury response compared with their WT counterparts.

STAT1 restrains early recruitment of neutrophils and tempers inflammatory responses to promote effective host defense during bacterial pneumonia

An inappropriate host inflammatory response to acute respiratory infection can lead to deleterious consequences such as lung injury (44, 46). To examine the early inflammatory response following KP infection, we evaluated the transcriptomic signature of murine lungs after 24 h of KP infection by bulk RNA-Seq. As expected, GSEA identified host defense, immunity, and IFN gene sets, in addition to neutrophil degranulation, as differentially upregulated between *Stat1*$^{-/-}$ and WT mice at 24 h (Fig. 2A). We also observed a prominent neutrophil signature early during infection with the loss of STAT1, even before increased bacterial burden in the lung or systemic dissemination was detected (Figs. 2B, 1A–1C). Among the upregulated neutrophil-associated genes were those associated with increased neutrophil function, such as *Camp*, *Mmp8*, *Ctsg*, *Mmp9*, *S100a8*, *S100a9*, *Csf3r*, and *Mmp25* (Fig. 2B). Consistent with the early, exaggerated inflammatory response observed by transcriptomic analysis, *Stat1*$^{-/-}$ mice displayed increased neutrophil infiltration into the lungs at 24 h after infection by flow cytometric analysis (Fig. 2C–2E). To distinguish between circulating neutrophils in the lung microvasculature versus neutrophils that have extravasated into the lung tissue interstitium, we injected CD45.2 i.v. to label all neutrophils contained within the vascular space immediately prior to lung harvest (42). Although circulating CD45.2^{pos} Ly6G^{+} neutrophil numbers were similar between WT and *Stat1*$^{-/-}$ mice (Fig. 2F), the numbers of extravascular CD45.2^{neg} Ly6G^{+} neutrophils were increased in the lungs of *Stat1*$^{-/-}$ mice by 24 h (Fig. 2G). Thus, *Stat1*$^{-/-}$ mice show an early, exaggerated neutrophilic inflammatory response in the lungs that precedes a difference in local or systemic bacterial burden with subsequent increases in proinflammatory cytokine and chemokine levels in the lungs at 48 and 72 h after infection (Supplemental Fig. 1H–1M).

Myeloid cell STAT1 is dispensable for pulmonary host defense against KP infection

Although increased neutrophils and activity were observed in the lung and at 24 h after infection, they were unable to clear KP infection in *Stat1*$^{-/-}$ mice. To understand whether this phenomenon was due to the absence of STAT1 expression in myeloid cells, including neutrophils, we used LysM$^{Cre/WT}$;*Stat1*$^{fl/fl}$ mice to remove STAT1 in only the myeloid cell lineage (Fig. 3). Surprisingly, we found no significant difference in bacterial burden in the lung, liver, or kidney or any notable differences in BALF PMN cells within LysM$^{Cre/WT}$;*Stat1*$^{fl/fl}$ mice compared with their WT littermates (Fig. 3A–3D). Additionally, we did not observe any difference in the phagocytic uptake of KP by WT and *Stat1*$^{-/-}$ BMDMs (Supplemental Fig. 1N). Although myeloid cells are essential for host defense, our data suggest a myeloid cell STAT1-extrinsic mechanism that is involved in the control of KP infection.

Circulating Th17 cells are present in the lungs of KP-infected *Stat1*$^{-/-}$ mice early during infection

To determine the role of STAT1 in regulating other cell types that may impact neutrophil behavior in the lung during KP infection, we performed scRNAseq analysis using lungs from WT and *Stat1*$^{-/-}$ mice following removal of neutrophils with anti-Ly6G microbeads (Fig. 4). Surprisingly, KP-infected *Stat1*$^{-/-}$ mice revealed an expansion of T cells in lung tissue at an early time point of 24 h (Fig. 4A). In contrast to the *Cd14*-expressing monocyte population, where no differences were observed between the groups (Fig. 4B), both *Cd8*- and *Cd4*-expressing T cell populations were increased in *Stat1*$^{-/-}$ mouse lungs at 24 h (Fig. 4C, 4D). Specifically, although *Cd4*-expressing T cells were not the main transcribers of *il17a*, *c*, *d*, *and f* in the WT group at 24 h following KP infection, *Cd4*-expressing T cells were the main transcribers of *il17a* in the lungs of *Stat1*$^{-/-}$ mice (Fig. 4E, 4F). GSEA also showed enhanced T cell pathways as upregulated in bulk RNA-seq of *Stat1*$^{-/-}$ mouse lungs, some of which were relevant to CD4^{+}αβTCR^{+} T cells, such as the CD4-positive, αβ T cell activation pathway (nominal p value <0.05) (Supplemental Table I).

Given these findings, we next examined CD4 and CD8 T cells in the lungs of WT and *Stat1*$^{-/-}$ mice (Fig. 5). Although the total numbers of CD4^{+} T cells were similar between WT and *Stat1*$^{-/-}$ mice, we observed increased IL-17–producing αβTCR^{+} CD4^{+} T cells in the lungs of *Stat1*$^{-/-}$ mice at 24 h after infection compared with WT mice (Fig. 5A). Although not significantly different, *Stat1*$^{-/-}$ mouse lungs displayed overall higher numbers of Th17 cells than WT lungs even with a noninfectious trigger (i.e., vehicle administration), suggesting that STAT1 tempers nonspecific T cell accumulation (Fig. 5A). In contrast to Th17 cells, γδ T cells showed similar numbers in both WT and *Stat1*$^{-/-}$ mice following infection but were detectable in lower numbers than αβTCR^{+} CD4^{+} T cells observed in *Stat1*$^{-/-}$ mice (Fig. 5B). Total CD8^{+} T cells were detectable in the lungs early after KP infection, but these T cell subsets were not producers of IL-17 (Supplemental Fig. 2A). We wondered if the accumulation of Th17 cells early after infection could be the consequence of a memory response by tissue-resident T cells from a prior KP infection. However, we did not find elevated anti-KP IgG titers in these mice, suggesting that a memory response did not drive accumulation of Th17 cells (Supplemental Fig. 2B). We also assessed the possibility that unknown baseline viral infection induced an IL-17 response in *Stat1*$^{-/-}$ mice, but we did not find any significant viral reads present in the scRNAseq data Viral-Track, an algorithm to identify viruses from scRNAseq raw data (data not shown) (47). Moreover, i.v. CD45.2 labeling indicated that the lung CD4^{+} T cells originated from the circulation rather than being tissue resident (Supplemental Fig. 2C, 2D). Furthermore, we also found that IL-17–producing αβTCR^{+} T cells do not exhibit markers

https://doi.org/10.4049/immunohorizons.2300104

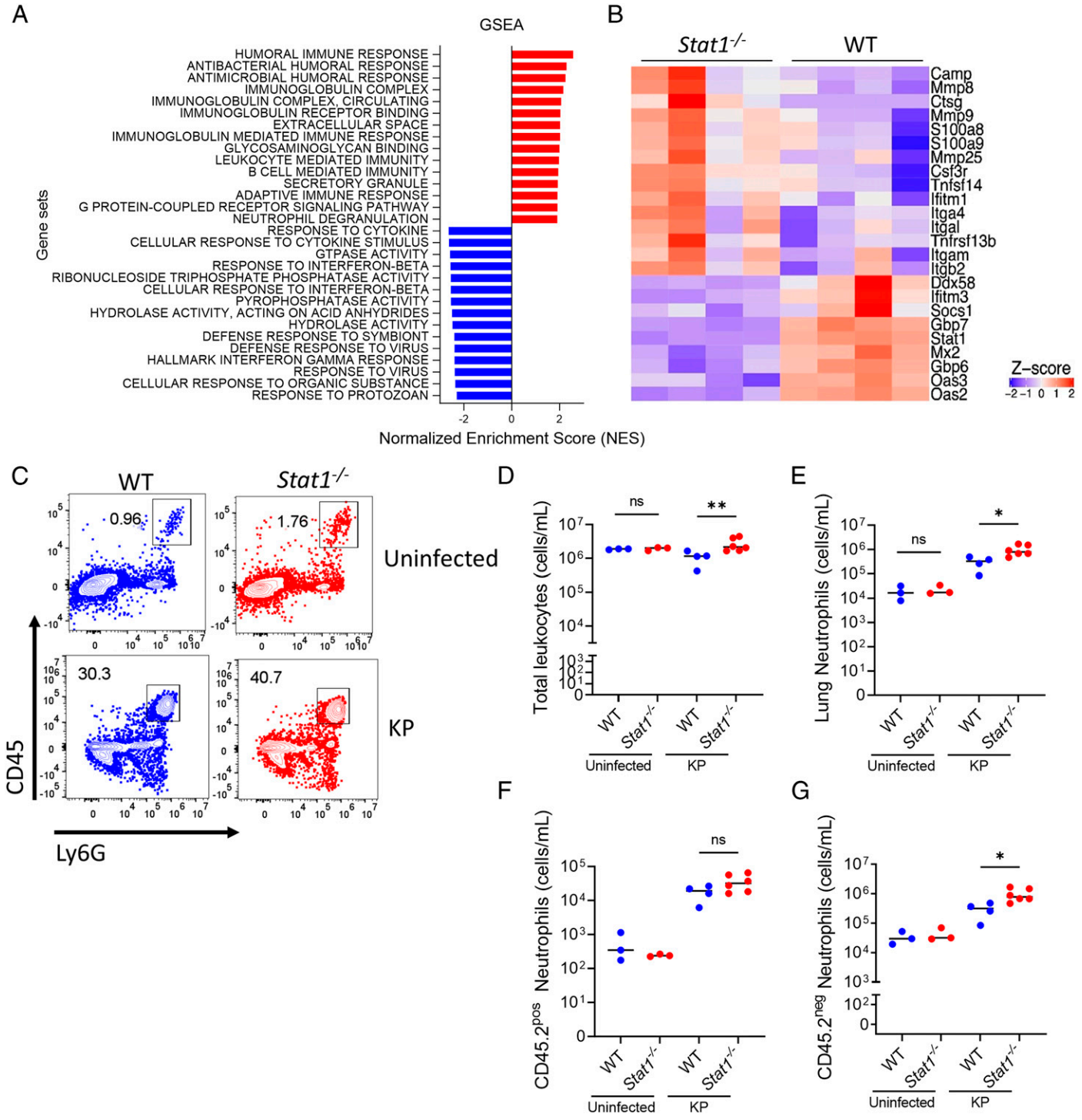

FIGURE 2.

An early neutrophil transcriptomic signature and increased neutrophil recruitment in *Stat1*$^{-/-}$ mice precedes impairments in host control of KP infection in the lung. Mice were infected intratracheally with 10^3 CFU KP bacteria, and lungs were harvested after 24 h. (**A**) GSEA of differentially expressed genes upregulated in the lungs of *Stat1*$^{-/-}$ mice relative to WT mice at 24 h after infection. Top 15 upregulated (red) and downregulated (blue) gene sets are shown along with their normalized enrichment score. (**B**) Heat map illustrating relative gene expression of selected genes across individual replicates at 24 h after infection from bulk RNA-Seq. Transcript counts were normalized using DESeq2, and z-scores are shown. Red denotes increased expression; blue indicates decreased expression. Each row and column represent one gene and an individual sample, respectively. Genes are ordered according to their differential expression between *Stat1*$^{-/-}$ and WT samples. (**C**) Representative FACS plot demonstrating CD45$^+$ Ly6G$^+$ lung neutrophils. (**D**) Total leukocyte counts are shown (cells/ml) using flow cytometric analysis. (**E**) Lung ***(Continued)***

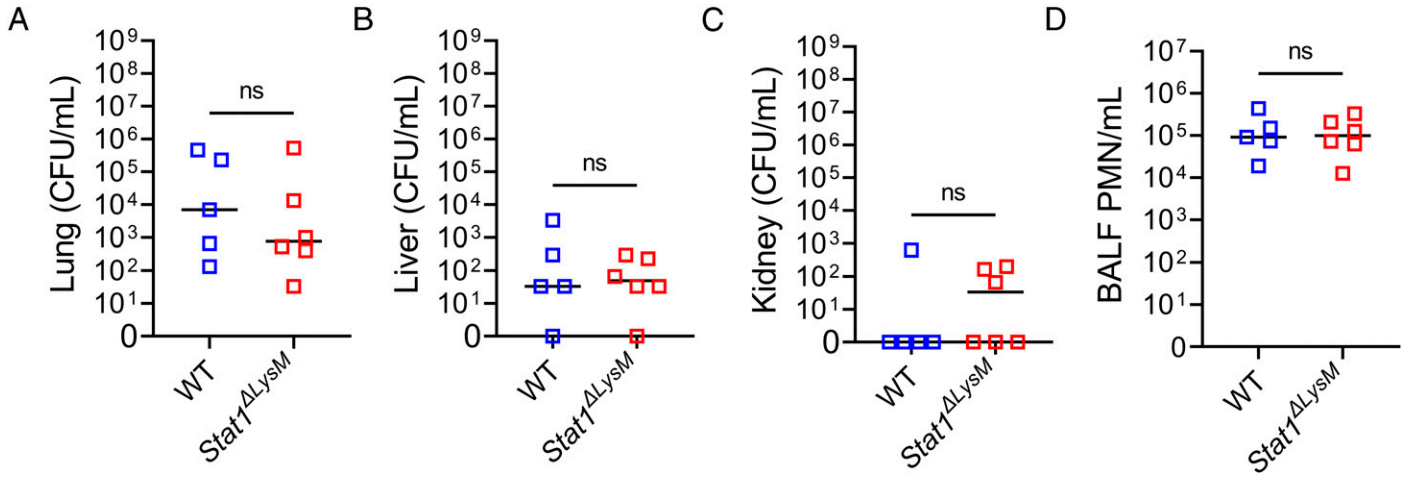

FIGURE 3.

Myeloid cell STAT1 is dispensable for pulmonary host defense against KP infection. LysM$^{Cre/WT}$;*Stat1*$^{fl/fl}$ mice and WT littermates (LysM$^{WT/WT}$;*Stat1*$^{fl/fl}$) were administered 10^3 CFU KP intratracheally, and tissues were harvested at 48 h for CFU enumeration in the (**A**) lung, (**B**) liver, and (**C**) kidney. (**D**) BALF PMN cells/ml were measured at 48 h after infection. Each dot represents an individual mouse. Horizontal lines indicate median values. Significance was assessed with Mann–Whitney *U* tests.

consistent with tissue-resident memory cells in WT or *Stat1*$^{-/-}$ mice (Supplemental Fig. 2E). Taken together, these findings suggest a dysregulated inflammatory response characterized by increased circulating IL-17–producing CD4$^+$ T cells as a potential mechanism for impaired host defense in *Stat1*$^{-/-}$ mice.

STAT1 prevents dysregulated CD4$^+$ T cell responses in the lungs

IL-17 plays a critical role in pulmonary host defense against extracellular bacterial infections, including KP (23, 24). However, it is not known whether Th17 skewing mediated by the loss of STAT1 can lead to defective host defense following bacterial lung infection. When total IL-17 signaling was inhibited using an anti–IL-17RC neutralizing Ab in *Stat1*$^{-/-}$ mice, the effect of global IL-17 antagonism proved deleterious with impaired lung bacterial burden and increased dissemination to the liver and kidney in *Stat1*$^{-/-}$ mice (Fig. 6A–6C). To investigate whether CD4$^+$ T cells contribute to impaired pulmonary host defense in *Stat1*$^{-/-}$ mice, we depleted CD4$^+$ T cells using an anti-CD4 Ab 48 h prior to KP infection (Fig. 6D–6F). We verified depletion of αβ TCR$^+$ CD4$^+$ T cells in the lung by flow cytometric analysis (Supplemental Fig. 3A). CD4 depletion improved lung bacterial burden at 48 h in *Stat1*$^{-/-}$ mice when compared with *Stat1*$^{-/-}$ mice treated with an IgG isotype control Ab (Fig. 6D). No differences in bacterial burden were observed in the liver (Fig. 6E) or kidney (Fig. 6F), implying that local KP control in the lung is key to preventing dissemination. T regulatory cells (Tregs) and Th17 cells share CD4$^+$ T cells as a precursor (48), and Th17 skewing can impair Treg differentiation during microbial infection (49). However, by scRNAseq, *Foxp3*-expressing Tregs in *Stat1*$^{-/-}$ mice were not substantially different from those in WT mice at 24 h after infection (Supplemental Fig. 3B). Interestingly, *Tbx21* and *Rorc* are Th1 and Th17 markers in the CD4 T cell population, respectively, that were increased in the *Stat1*$^{-/-}$ mice lungs at 24 h after infection (Supplemental Fig. 3C). Th1 and Th17 cells can have reciprocal relationships, and the inability of the Th1 cytokine IFN-γ to transduce signal in *Stat1*$^{-/-}$ mice may contribute to Th17 skewing. We also examined whether deletion of STAT1 could alter the expression of other *Stat* genes, such as *Stat3*, but no significant differences were noted (Supplemental Fig. 3D). It is also possible that CD4 depletion improves pulmonary host defense by increasing NK numbers via altering the balance of Tregs (50). However, CD4 depletion caused no significant impact on NK cell numbers in the lung (Supplemental Fig. 3E). Taken together, these findings suggest that STAT1 constrains pathogenic CD4$^+$ T cell responses in the lung to enhance pulmonary host defense during severe bacterial infection.

DISCUSSION

We previously reported that STAT1 dysregulation early during KP infection promotes the transition from local infection to extrapulmonary sepsis (8). In this study, we examined the

CD45$^+$ Ly6G$^+$ neutrophils (cells/ml) are increased in *Stat1*$^{-/-}$ mice by 24 h compared with WT mice. (**F**) In separate experiments, circulating CD45.2^{pos} Ly6G$^+$ neutrophil counts (cells/ml) are similar between WT and *Stat1*$^{-/-}$ mice at 24 h and (**G**) CD45.2^{neg} Ly6G$^+$ neutrophils (cells/ml) that have migrated into the lung interstitium and/or airspaces are increased in *Stat1*$^{-/-}$ mice by 24 h compared with WT mice. Each dot represents an individual mouse. Blue dots, WT mice; red dots, *Stat1*$^{-/-}$ mice. Horizontal lines indicate median values. *$p < 0.05$, **$p < 0.01$ from Mann–Whitney *U* tests.

https://doi.org/10.4049/immunohorizons.2300104

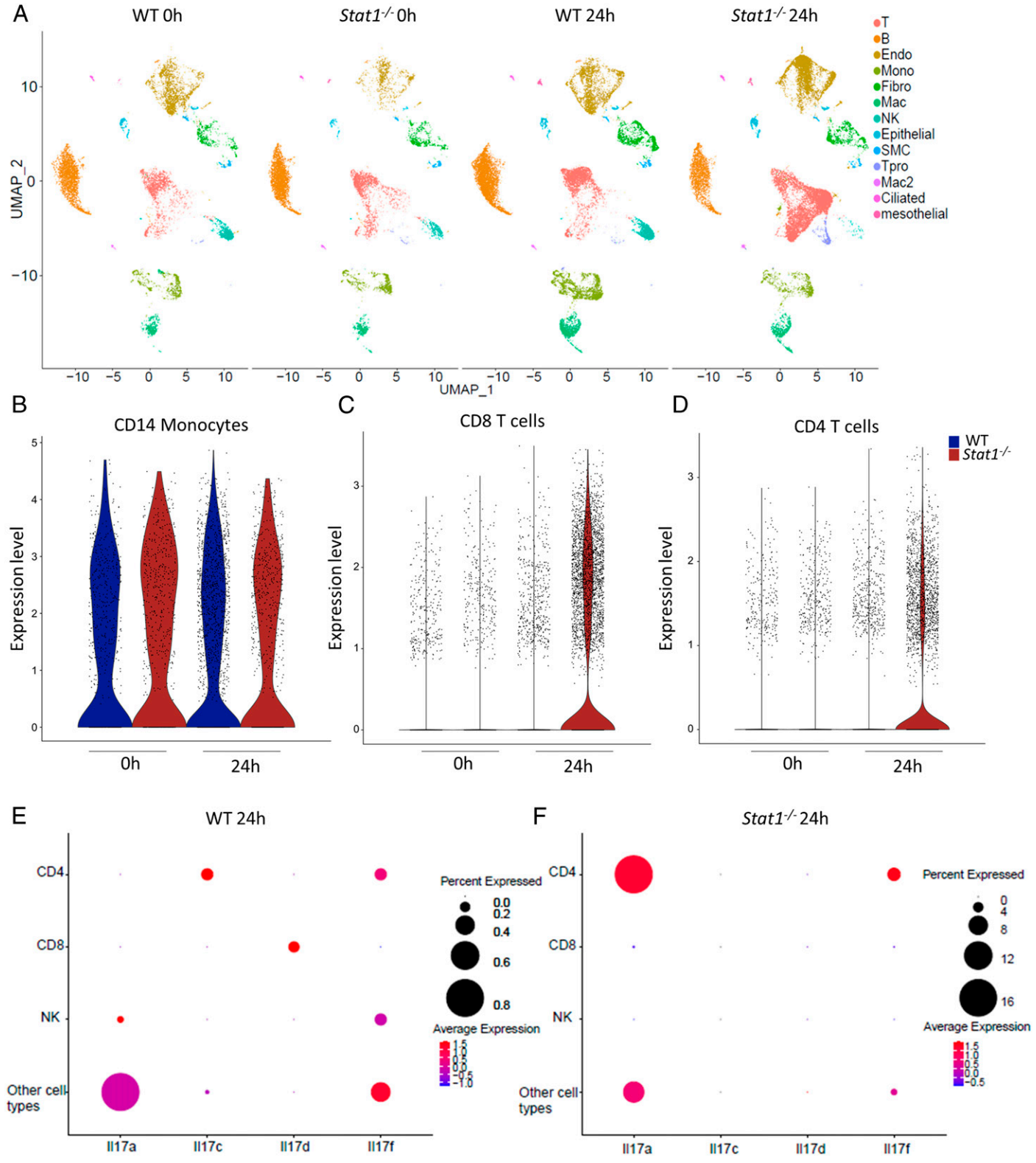

FIGURE 4.

scRNAseq reveals early T cell profile in KP-infected *Stat1*$^{-/-}$ mice. scRNAseq using the 10× Genomics platform was performed on lung tissue from neutrophil-depleted whole-lung tissues from WT and *Stat1*$^{-/-}$ mice at 0 and 24 h after infection. (**A**) Using clustering analysis, Uniform Manifold Approximation and Projection plots of 13 unique cell clusters in the four different groups were identified: T cells (T), B cells (B), endothelial cells (Endo), monocytes (Mono), fibroblasts (Fibro), macrophages (Mac), NK cells (NK), epithelial cells, smooth muscle cells (SMCs), ***(Continued)***

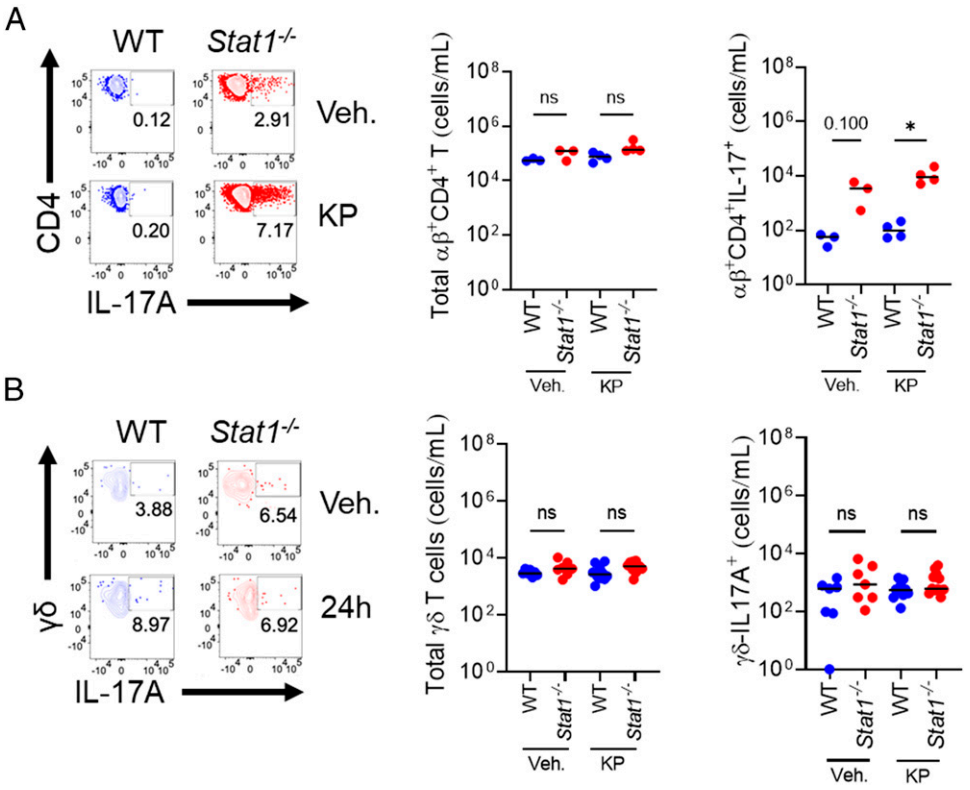

FIGURE 5.
Increased IL-17–producing $CD3^+$ $CD4^+$ $\alpha\beta TCR^+$ T cells in the lungs of *Stat1*$^{-/-}$ mice early after KP infection. Mice were administered PBS (vehicle) or 10^3 CFU KP delivered intratracheally. Lungs were harvested at 24 h after infection, and flow cytometric analysis was performed. (**A**) Total $\alpha\beta TCR^+$ $CD4^+$ T cells and $CD4^+$ IL-17^+ T cells (cells/ml) are shown. (**B**) Flow cytometric analysis of total γδ T cells and IL-17–producing γδ T cells (cells/ml) are shown. Data are combined from two independent experiments, with each dot representing an individual mouse. Horizontal lines indicate median values. *$p < 0.05$ from Mann–Whitney *U* test.

mechanistic link between global loss of STAT1 and dysregulated host defense during pneumonia-induced sepsis. In the absence of STAT1, we found an early neutrophil-dominant transcriptomic signature and accumulation of neutrophils in the lung parenchyma that preceded differences in lung bacterial burden and extrapulmonary dissemination. *Stat1*$^{-/-}$ mice developed increased lung microvascular permeability, exaggerated neutrophilic inflammation, and widespread bacterial dissemination. Conditional deletion of STAT1 in myeloid cells failed to show differences in pulmonary host defense when compared with WT littermates, indicating that STAT1 in myeloid cells is dispensable for KP host defense. Using scRNAseq, we observed an increase in *Cd4* and *Cd8* T cell signatures at 24 h following infection, with skewing of *Il17a* producing *Cd4* T cells in *Stat1*$^{-/-}$ mouse lungs. By flow cytometric analysis of lung tissue, we confirmed an increase in the numbers of IL-17–producing $CD4^+$ T cells in the lungs of *Stat1*$^{-/-}$ mice. IL-17–producing γδ T cells, although detectable in the lungs, did not increase in number following KP infection, nor were they differentially abundant between WT and *Stat1*$^{-/-}$ mice. $CD8^+$ T cells were also detectable in the lung but were not IL-17–producing. Notably, the increase in Th17 cells in the lung was not due to preexisting immunity against KP and was consistent with circulating rather than tissue-resident cells. Our observations suggest that the early rise of Th17 cells recruited to the lung in *Stat1*$^{-/-}$ mice in response to infection with KP appears to be TCR independent. Last, we found that blocking total IL-17 signaling was detrimental, whereas depletion of $CD4^+$ T cells was protective, in pulmonary host defense. These findings indicate that STAT1 restricts nonspecific T cell activation during KP infection, thereby improving lung host defense against KP and preventing infection-induced immunopathology.

Our study adds to the growing literature examining the link between STAT1 signaling and critical immune effectors, such as Th17 cells. Others have shown that lack of tonic IFN signaling leads to expansion of Th17 cells in *Stat1*$^{-/-}$ mice, causing them to develop myeloid hyperplasia and splenic accumulation of hematopoietic stem cells (7). The same study also found that circulating $CD4^+$ T cells and NK cells produce elevated levels of IL-17A in *Stat1*$^{-/-}$ mice (7). Others have also found that *Stat1*$^{-/-}$ mice developed increased levels of Th17 cells during influenza and bacterial pneumonia coinfection (29). In our study, *Stat1*$^{-/-}$ mice display a nonsignificant elevation of IL-17–producing $CD4^+$ T cells in the lung vasculature under homeostasis. Following KP infection, Th17 cells increase significantly, presumably in response to a heightened proinflammatory environment enriched with neutrophils. We suggest that the Th17 cells observed early during KP infection are preexisting T cells in the

proinflammatory T cells (Tpro), type 2 macrophages (Mac2), ciliated cells, and mesothelial cells. Violin plots across all groups display no unique expansion in (**B**) CD14 monocytes, but they do show an increase in (**C**) CD8 and (**D**) CD4 T cells in *Stat1*$^{-/-}$ mice at 24 h after infection. Dot plots of (**E**) WT and (**F**) *Stat1*$^{-/-}$ mice at 24 h postinfection display differences in IL-17 family gene (i.e., *il17a, c, d, f*) expression among cells.

https://doi.org/10.4049/immunohorizons.2300104

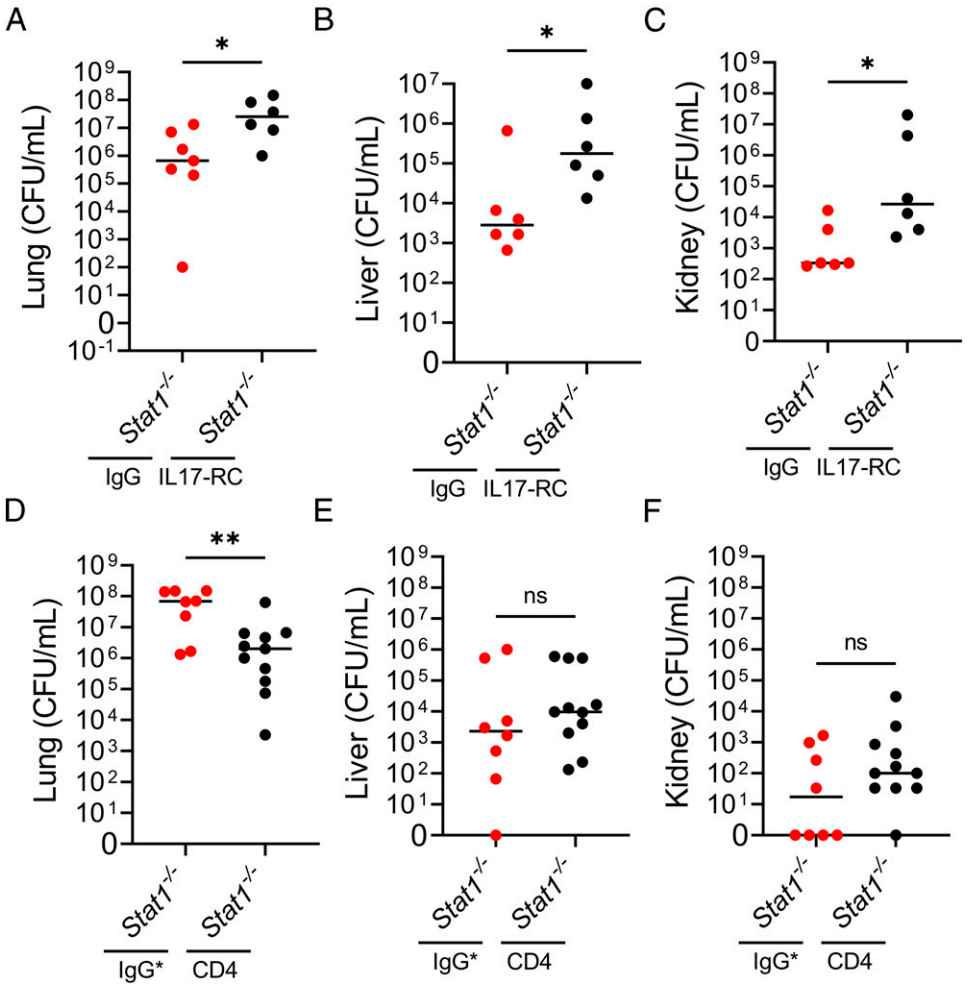

FIGURE 6.

Blocking total IL-17 signaling worsens lung bacterial burden, whereas depletion of $CD4^+$ T cells improves host defense in *Stat1*$^{-/-}$ mice. *Stat1*$^{-/-}$ mice were treated with IL-17RC neutralizing Ab (50-μg dose) (**A**–**C**), anti-CD4 Ab (200-μg dose) (**D**–**F**), or respective IgG (IgG and IgG*) isotype control Abs (A–F). IL-17RC neutralizing Ab was administered 6 h after KP infection, whereas CD4 Ab was administered 48 h prior to KP infection. Tissues were harvested at 48 h after KP infection, and CFUs were quantified in the (A and D) lung, (B and E) liver, and (C and F) kidney. Each dot represents an individual mouse. (D–F) Data represent two independent experiments. Horizontal lines indicate median values. *$p < 0.05$, **$p < 0.01$ from Mann–Whitney *U* tests.

circulation and speculate that their recruitment and activation in the lungs is from the local cytokine milieu, which these cells further amplify. In contrast, by scRNAseq, we did not observe an increased *Il17a*-expressing NK cell signature in the lungs of *Stat1*$^{-/-}$ mice after infection. Additionally, targeting total IL-17 signaling with anti–IL-17RC Ab in our study worsened rather than improved pulmonary host defense. Our findings are consistent with other prior literature demonstrating the essential role of IL-17 in defense against extracellular bacteria such as KP (24, 25, 51) and invoke the important protective role of γδ T cells that are resident in the lung, whereas mediators from $CD4^+$ T cell activity during STAT1 deficiency may be pathogenic. This idea is supported by our findings that depletion of $CD4^+$ T cells in *Stat1*$^{-/-}$ mice aids in pulmonary host defense against KP lung infection.

Our findings explore the role of T cell homeostasis and how STAT1 keeps nonspecific T cell activation in check during infection and injury. We found no evidence for elevated IgG titers in response to KP, which would have suggested prior KP infection, or that increased IL-17–producing $CD4^+$ T cells were tissue-resident memory T cells. The early recruitment of circulating Th17 cells even following vehicle PBS administration lends further support to the idea that STAT1 mitigates nonspecific T cell activation. Moreover, our finding that acute depletion of $CD4^+$ T cells in *Stat1*$^{-/-}$ mice improved host defense also supports the pathogenic phenotype of these cells. Others have reported that *Stat1*$^{-/-}$ mice show myeloid hyperplasia (7, 34, 52) and hematopoietic stem cell and progenitor cell accumulation in secondary lymphoid organs (7). Deletion of *Il17ra* in *Stat1*$^{-/-}$ mice corrected these abnormalities, implying that the inflammatory phenotype is driven mainly by a pathogenic IL-17 state (7). Precisely how Th17 cells are driven to a pathogenic state in the absence of tonic IFN signaling remains unclear. Although *Stat1* deficiency produces a state of severe immunosuppression, our findings show an early and vigorous neutrophilic inflammation that precedes bacterial replication and dissemination following KP infection. We speculate that mediators from CD4 T cell activity in the setting of STAT1 deficiency amplify neutrophil recruitment, activation, and survival. Specifically, Th17 cells promote the secretion of IL-1β, GM-CSF, G-CSF, and CXCL1 by epithelial, endothelial, and other stromal cells (53). In our model, we observed increased GM-CSF, CXCL1, and G-CSF levels in lung tissue at 48 and 72 h as well as IL-1β at 48 h, further supporting the idea of increased neutrophil recruitment

and survival. Although this may seem counterintuitive (i.e., excessive numbers of neutrophils coming in early with delayed impairments in host defense), excessive inflammation can be harmful in human pneumonia, where the use of steroids has been shown to improve survival (54). Moreover, fludarabine is a specific STAT1 inhibitor (55) and used in conditioning regimens prior to hematopoietic stem cell transplant for certain hematologic malignancies (56–59). Fludarabine causes profound and prolonged immunosuppression, and it remains to be seen whether these patients develop nonspecific T cell activation and delayed lung injury in the setting of infectious pneumonia and immune reconstitution.

One limitation of our study is that global STAT1 depletion may impose defects in other expressing cell types in addition to $CD4^+$ T cells. Nonetheless, we were able to demonstrate the pathogenic role of $CD4^+$ T cells in the lung following KP infection of *Stat1*$^{-/-}$ mice. This CD4 depletion did not significantly impact NK cells, which are often suppressed by Tregs (50), and the lungs of *Stat1*$^{-/-}$ mice did not show NK cells as major expressors of *Il17a*. It is important to note that our data showed enrichment in neutrophils by 24 h, as well as Th17-dependent pathway enrichment by 48 h, as noted by bulk RNA-seq GSEA. In agreement with our flow cytometry data, we showed that neutrophils are recruited into the lung interstitium by 24 h, whereas Th17 cells are present in the circulation at 24 h but have not yet entered the lung parenchyma. This feature may suggest neutrophil inflammation as one driving force for Th17 cell accumulation, because others have shown that IL-17 activation is mediated by neutrophil accumulation during parasitic infection (60). We speculate Th17 cells then further amplify neutrophil recruitment, activation, and survival that create a cycle of excessive inflammation and immunopathology. Our data also suggest that not all IL-17–producing cells are alike and that Th17 cells can exhibit functional plasticity even during acute bacterial infection regulated by STAT1.

In summary, our study focuses on the role of STAT1 in pulmonary host defense during acute bacterial pneumonia. STAT1, through tonic IFN signaling, acts to maintain T cell quiescence under homeostatic conditions (7). We demonstrate the relevance of STAT1-regulated T cell quiescence in pulmonary host defense and prevention of excessive neutrophilic inflammation that can lead to lung injury. A better understanding of how STAT1 prevents the propensity of T cells toward nonspecific activation may aid future work focused on targeted therapies and management of severe infections that lead to a dysregulated host response.

DISCLOSURES

The authors have no financial conflicts of interest.

REFERENCES

1. Ashurst, J. V., and A. Dawson. 2023. *Klebsiella* pneumonia. In *StatPearls*. StatPearls Publishing, Treasure Island, FL.
2. Bengoechea, J. A., and J. Sa Pessoa. 2019. *Klebsiella pneumoniae* infection biology: living to counteract host defences. *FEMS Microbiol. Rev.* 43: 123–144.
3. Schurr, J. R., E. Young, P. Byrne, C. Steele, J. E. Shellito, and J. K. Kolls. 2005. Central role of Toll-like receptor 4 signaling and host defense in experimental pneumonia caused by Gram-negative bacteria. *Infect. Immun.* 73: 532–545.
4. Ramana, C. V., M. Chatterjee-Kishore, H. Nguyen, and G. R. Stark. 2000. Complex roles of Stat1 in regulating gene expression. *Oncogene* 19: 2619–2627.
5. Au-Yeung, N., R. Mandhana, and C. M. Horvath. 2013. Transcriptional regulation by STAT1 and STAT2 in the interferon JAK-STAT pathway. *JAKSTAT* 2: e23931.
6. Platanias, L. C. 2005. Mechanisms of type-I- and type-II-interferon-mediated signalling. *Nat. Rev. Immunol.* 5: 375–386.
7. Marié, I. J., L. Brambilla, D. Azzouz, Z. Chen, G. V. Baracho, A. Arnett, H. S. Li, W. Liu, L. Cimmino, P. Chattopadhyay, et al. 2021. Tonic interferon restricts pathogenic IL-17-driven inflammatory disease via balancing the microbiome. *eLife* 10: e68371.
8. Olonisakin, T. F., T. Suber, S. Gonzalez-Ferrer, Z. Xiong, H. F. Peñaloza, R. van der Geest, Y. Xiong, D. O. Osei-Hwedieh, J. Tejero, M. R. Rosengart, et al. 2021. Stressed erythrophagocytosis induces immunosuppression during sepsis through heme-mediated STAT1 dysregulation. *J. Clin. Invest.* 131: e137468.
9. Xu, Q., M. Xie, X. Liu, H. Heng, H. Wang, C. Yang, E. W.-C. Chan, R. Zhang, G. Yang, and S. Chen. 2023. Molecular mechanisms underlying the high mortality of hypervirulent *Klebsiella pneumoniae* and its effective therapy development. *Signal Transduct. Target. Ther.* 8: 221.
10. Lin, Y.-C., M.-C. Lu, C. Lin, M.-K. Chiang, M.-S. Jan, H.-L. Tang, H.-C. Liu, W.-L. Lin, C.-Y. Huang, C.-M. Chen, and Y.-C. Lai. 2013. Activation of IFN-γ/STAT/IRF-1 in hepatic responses to *Klebsiella pneumoniae* infection. *PLoS One* 8: e79961.
11. Poe, S. L., M. Arora, T. B. Oriss, M. Yarlagadda, K. Isse, A. Khare, D. E. Levy, J. S. Lee, R. K. Mallampalli, Y. R. Chan, et al. 2013. STAT1-regulated lung MDSC-like cells produce IL-10 and efferocytose apoptotic neutrophils with relevance in resolution of bacterial pneumonia. *Mucosal Immunol.* 6: 189–199.
12. Saha, D., and S. Kundu. 2021. A molecular interaction map of *Klebsiella pneumoniae* and its human host reveals potential mechanisms of host cell subversion. *Front. Microbiol.* 12: 613067.
13. Martignoni, A., J. Tschöp, H. S. Goetzman, L. G. Choi, M. D. Reid, J. A. Johannigman, A. B. Lentsch, and C. C. Caldwell. 2008. CD4-expressing cells are early mediators of the innate immune system during sepsis. *Shock* 29: 591–597.
14. Ma, Y., Y. Zhang, and L. Zhu. 2021. Role of neutrophils in acute viral infection. *Immun. Inflamm. Dis.* 9: 1186–1196.
15. Delgado-Ramirez, Y., I. Baltazar-Perez, Y. Martinez, B. E. Callejas, I. Medina-Andrade, J. E. Olguín, N. L. Delgado-Buenrostro, Y. I. Chirino, L. I. Terrazas, and S. Leon-Cabrera. 2021. STAT1 is required for decreasing accumulation of granulocytic cells via IL-17 during initial steps of colitis-associated cancer. *Int. J. Mol. Sci.* 22: 7695.
16. Thoeni, C., E. A. Hamilton, A. Elkadri, R. Murchie, K. Fiedler, A. Ovadia, N. Sharfe, B. Ngan, E. Cutz, A. Nahum, et al. 2016. The effects of STAT1 dysfunction on the gut. *LymphoSign J.* 3: 19–33.
17. Sharfe, N., A. Nahum, A. Newell, H. Dadi, B. Ngan, S. L. Pereira, J.-A. Herbrick, and C. M. Roifman. 2014. Fatal combined immunodeficiency associated with heterozygous mutation in STAT1. *J. Allergy Clin. Immunol.* 133: 807–817.
18. Park, J., M.-J. Son, C.-C. Ho, S.-H. Lee, Y. Kim, J. An, and S.-K. Lee. 2022. Transcriptional inhibition of STAT1 functions in the nucleus alleviates Th1 and Th17 cell-mediated inflammatory diseases. [Published erratum appears in 2023 *Front. Immunol.* 14: 1307575.] *Front. Immunol.* 13: 1054472.
19. Boehmer, D. F. R., L. M. Koehler, T. Magg, P. Metzger, M. Rohlfs, J. Ahlfeld, A. Rack-Hoch, K. Reiter, M. H. Albert, S. Endres, et al.

2020. A novel complete autosomal-recessive STAT1 LOF variant causes immunodeficiency with hemophagocytic lymphohistiocytosis-like hyperinflammation. *J. Allergy Clin. Immunol. Pract.* 8: 3102–3111.
20. Burns, C., A. Cheung, Z. Stark, S. Choo, L. Downie, S. White, R. Conyers, and T. Cole. 2016. A novel presentation of homozygous loss-of-function STAT-1 mutation in an infant with hyperinflammation—a case report and review of the literature. *J. Allergy Clin. Immunol. Pract.* 4: 777–779.
21. Zhang, W., X. Chen, G. Gao, S. Xing, L. Zhou, X. Tang, X. Zhao, and Y. An. 2021. Clinical relevance of gain- and loss-of-function germline mutations in STAT1: a systematic review. *Front. Immunol.* 12: 654406.
22. Boisson-Dupuis, S., X.-F. Kong, S. Okada, S. Cypowyj, A. Puel, L. Abel, and J.-L. Casanova. 2012. Inborn errors of human STAT1: allelic heterogeneity governs the diversity of immunological and infectious phenotypes. *Curr. Opin. Immunol.* 24: 364–378.
23. Mills, K. H. G. 2023. IL-17 and IL-17-producing cells in protection versus pathology. *Nat. Rev. Immunol.* 23: 38–54.
24. McGeachy, M. J., D. J. Cua, and S. L. Gaffen. 2019. The IL-17 family of cytokines in health and disease. *Immunity* 50: 892–906.
25. Ye, P., F. H. Rodriguez, S. Kanaly, K. L. Stocking, J. Schurr, P. Schwarzenberger, P. Oliver, W. Huang, P. Zhang, J. Zhang, et al. 2001. Requirement of interleukin 17 receptor signaling for lung CXC chemokine and granulocyte colony-stimulating factor expression, neutrophil recruitment, and host defense. *J. Exp. Med.* 194: 519–527.
26. Crowe, C. R., K. Chen, D. A. Pociask, J. F. Alcorn, C. Krivich, R. I. Enelow, T. M. Ross, J. L. Witztum, and J. K. Kolls. 2009. Critical role of IL-17RA in immunopathology of influenza infection. *J. Immunol.* 183: 5301–5310.
27. Chen, K., J. P. McAleer, Y. Lin, D. L. Paterson, M. Zheng, J. F. Alcorn, C. T. Weaver, and J. K. Kolls. 2011. Th17 cells mediate clade-specific, serotype-independent mucosal immunity. *Immunity* 35: 997–1009.
28. Arbelaez, C. A., P. Palle, J. Charaix, and E. Bettelli. 2022. STAT1 signaling protects self-reactive T cells from control by innate cells during neuroinflammation. *JCI Insight* 7: e148222.
29. Lee, B., R. Gopal, M. L. Manni, K. J. McHugh, S. Mandalapu, K. M. Robinson, and J. F. Alcorn. 2017. STAT1 is required for suppression of type 17 immunity during influenza and bacterial superinfection. *Immunohorizons* 1: 81–91.
30. Varikuti, S., S. Oghumu, M. Elbaz, G. Volpedo, D. K. Ahirwar, P. C. Alarcon, R. H. Sperling, E. Moretti, M. S. Pioso, J. Kimble, et al. 2017. STAT1 gene deficient mice develop accelerated breast cancer growth and metastasis which is reduced by IL-17 blockade. *OncoImmunology* 6: e1361088.
31. Leon-Cabrera, S., A. Vázquez-Sandoval, E. Molina-Guzman, Y. Delgado-Ramirez, N. L. Delgado-Buenrostro, B. E. Callejas, Y. I. Chirino, C. Pérez-Plasencia, M. Rodríguez-Sosa, J. E. Olguín, et al. 2018. Deficiency in STAT1 signaling predisposes gut inflammation and prompts colorectal cancer development. *Cancers (Basel)* 10: 341.
32. Meier, S. L., A. T. Satpathy, and D. K. Wells. 2022. Bystander T cells in cancer immunology and therapy. *Nat. Can.* 3: 143–155.
33. Sun, C., R. Mezzadra, and T. N. Schumacher. 2018. Regulation and function of the PD-L1 checkpoint. *Immunity* 48: 434–452.
34. Kye, Y.-C., G.-W. Lee, S.-W. Lee, Y.-J. Ju, H.-O. Kim, C.-H. Yun, and J.-H. Cho. 2021. STAT1 maintains naïve $CD8^+$ T cell quiescence by suppressing the type I IFN-STAT4-mTORC1 signaling axis. *Sci. Adv.* 7: eabg8764.
35. Ito, R., Y. Shindo, D. Kobayashi, M. Ando, W. Jin, J. Wachino, K. Yamada, K. Kimura, T. Yagi, Y. Hasegawa, and Y. Arakawa. 2015. Molecular epidemiological characteristics of *Klebsiella pneumoniae* associated with bacteremia among patients with pneumonia. *J. Clin. Microbiol.* 53: 879–886.
36. van der Geest, R., H. Fan, H. F. Peñaloza, W. G. Bain, Z. Xiong, N. Kohli, E. Larson, M. L. G. Sullivan, J. M. Franks, D. B. Stolz, et al. 2023. Phagocytosis is a primary determinant of pulmonary clearance of clinical *Klebsiella pneumoniae* isolates. *Front. Cell. Infect. Microbiol.* 13: 1150658.
37. Matute-Bello, G., G. Downey, B. B. Moore, S. D. Groshong, M. A. Matthay, A. S. Slutsky, and W. M. Kuebler; Acute Lung Injury in Animals Study Group. 2011. An official American Thoracic Society workshop report: features and measurements of experimental acute lung injury in animals. *Am. J. Respir. Cell Mol. Biol.* 44: 725–738.
38. Pineda-Torra, I., M. Gage, A. de Juan, and O. M. Pello. 2015. Isolation, culture, and polarization of murine bone marrow-derived and peritoneal macrophages. *Methods Mol. Biol.* 1339: 101–109.
39. Reimand, J., R. Isserlin, V. Voisin, M. Kucera, C. Tannus-Lopes, A. Rostamianfar, L. Wadi, M. Meyer, J. Wong, C. Xu, et al. 2019. Pathway enrichment analysis and visualization of omics data using g:Profiler, GSEA, Cytoscape and EnrichmentMap. *Nat. Protoc.* 14: 482–517.
40. Anders, S., and W. Huber. 2010. Differential expression analysis for sequence count data. *Genome Biol.* 11: R106.
41. Jakubzick, C., J. Helft, T. J. Kaplan, and G. J. Randolph. 2008. Optimization of methods to study pulmonary dendritic cell migration reveals distinct capacities of DC subsets to acquire soluble versus particulate antigen. *J. Immunol. Methods* 337: 121–131.
42. Pioli, K. T., and P. D. Pioli. 2023. Retro-orbital CD45 antibody labeling to evaluate antibody-secreting cell trafficking in mice. *STAR Protoc* 4: 102308.
43. Marchesi, V., and T. Rukavina. 2007. The kinetics of IL-17 production in the lungs and plasma of mice after intratracheal infection with *Klebsiella pneumoniae*. *Crit. Care* 11(Suppl 4): P40.
44. Peñaloza, H. F., T. F. Olonisakin, W. G. Bain, Y. Qu, R. van der Geest, J. Zupetic, M. Hulver, Z. Xiong, M. W. Newstead, C. Zou, et al. 2021. Thrombospondin-1 restricts interleukin-36γ-mediated neutrophilic inflammation during *Pseudomonas aeruginosa* pulmonary infection. *MBio* 12: e03336-20.
45. Olonisakin, T. F. 2020. *Stressed Erythrophagocytosis as a Modifier of the Innate Immune Response to* Klebsiella pneumoniae. Dissertation, University of Pittsburgh, Pittsburgh, PA.
46. Peñaloza, H. F., L. P. Noguera, D. Ahn, O. P. Vallejos, R. M. Castellanos, Y. Vazquez, F. J. Salazar-Echegarai, L. González, I. Suazo, C. Pardo-Roa, et al. 2019. Interleukin-10 produced by myeloid-derived suppressor cells provides protection to carbapenem-resistant *Klebsiella pneumoniae* sequence type 258 by enhancing its clearance in the airways. *Infect. Immun.* 87: e00665-18.
47. Bost, P., A. Giladi, Y. Liu, Y. Bendjelal, G. Xu, E. David, R. Blecher-Gonen, M. Cohen, C. Medaglia, H. Li, et al. 2020. Host-viral infection maps reveal signatures of severe COVID-19 patients. *Cell* 181: 1475–1488.e12.
48. Lee, G. R. 2018. The balance of Th17 versus Treg cells in autoimmunity. *Int. J. Mol. Sci.* 19: 730.
49. Zheng, S. G. 2013. Regulatory T cells vs Th17: differentiation of Th17 versus Treg, are the mutually exclusive? *Am. J. Clin. Exp. Immunol.* 2: 94–106.
50. Pedroza-Pacheco, I., A. Madrigal, and A. Saudemont. 2013. Interaction between natural killer cells and regulatory T cells: perspectives for immunotherapy. *Cell. Mol. Immunol.* 10: 222–229.
51. Happel, K. I., P. J. Dubin, M. Zheng, N. Ghilardi, C. Lockhart, L. J. Quinton, A. R. Odden, J. E. Shellito, G. J. Bagby, S. Nelson, and J. K. Kolls. 2005. Divergent roles of IL-23 and IL-12 in host defense against *Klebsiella pneumoniae*. *J. Exp. Med.* 202: 761–769.
52. Porpaczy, E., S. Tripolt, A. Hoelbl-Kovacic, B. Gisslinger, Z. Bago-Horvath, E. Casanova-Hevia, E. Clappier, T. Decker, S. Fajmann, D. A. Fux, et al. 2018. Aggressive B-cell lymphomas in patients with myelofibrosis receiving JAK1/2 inhibitor therapy. [Published erratum appears in 2019 *Blood* 133: 768.] *Blood* 132: 694–706.
53. Weaver, C. T., C. O. Elson, L. A. Fouser, and J. K. Kolls. 2013. The Th17 pathway and inflammatory diseases of the intestines, lungs, and skin. *Annu. Rev. Pathol.* 8: 477–512.
54. Dequin, P.-F., F. Meziani, J.-P. Quenot, T. Kamel, J.-D. Ricard, J. Badie, J. Reignier, N. Heming, G. Plantefève, B. Souweine, et al;

CRICS-TriGGERSep Network. 2023. Hydrocortisone in severe community-acquired pneumonia. *N. Engl. J. Med.* 388: 1931–1941.
55. Frank, D. A., S. Mahajan, and J. Ritz. 1999. Fludarabine-induced immunosuppression is associated with inhibition of STAT1 signaling. *Nat. Med.* 5: 444–447.
56. Deeg, H. J. 2006. Transplant strategies for patients with myelodysplastic syndromes. *Curr. Opin. Hematol.* 13: 61–66.
57. Tan, Y. M., H. R. Fu, Y. Luo, J. M. Shi, X. J. Ye, Y. L. Zheng, H. W. Xiao, Y. X. Hu, and H. Huang. 2011. Haploidentical allogeneic haematopoietic stem cell transplantation as salvage therapy for engraftment failure after unrelated and autologous stem cell transplantation: a case report and review of the literature. *J. Int. Med. Res.* 39: 950–959.
58. Zang, D. Y., and H. J. Deeg. 2009. Allogeneic hematopoietic cell transplantation for patients with myelofibrosis. *Curr. Opin. Hematol.* 16: 140–146.
59. Luo, Y., C. Wang, Z. Du, C. Wang, Y. Wu, and A. Lei. 2023. Nitric oxide-producing polymorphonuclear neutrophils confer protection against *Chlamydia psittaci* in mouse lung infection. *J. Infect. Dis.* 228: 453–463.
60. Gonçalves-de-Albuquerque, S. D. C., R. Pessoa-E-Silva, L. A. M. Trajano-Silva, T. C. de Goes, R. C. S. de Morais, C. N. da C Oliveira, V. M. B. de Lorena, and M. de Paiva-Cavalcanti. 2017. The equivocal role of th17 cells and neutrophils on immunopathogenesis of leishmaniasis. *Front. Immunol.* 8: 1437.